RSC Advances

PAPER

View Article Online
View Journal | View Issue

Cite this: RSC Adv., 2015, 5, 99164

Poly(3,4-ethylenedioxythiophene)/nickel disulfide microspheres hybrid in energy storage and conversion cells†

Radha Mukkabla,[a] Melepurath Deepa*[a] and Avanish Kumar Srivastava[b]

The redox pseudocapacitive response of a hybrid material made up of NiS_2 microspheres embedded in a poly(3,4-ethylenedioxythiophene) or (PEDOT) layer is demonstrated for the first time. NiS_2 microspheres of 2 to 3.5 μm dimensions were synthesized by a hydrothermal route and after electropolymerization with the monomer, EDOT, an assembly of the PEDOT/NiS_2 hybrid was obtained on both rigid (stainless steel (SS) foil) and flexible (carbon (C)-fabric) current collectors. The synergy between NiS_2 microspheres (electrically conductive, and composed of flaky nanoparticles thus ensuring good electrolyte penetration) when hybridized with PEDOT, (which provides a robust scaffold for the microspheres to adhere to, acts as a conductive glue and prevents their aggregation) allows charge storage and release by faradaic reactions. Symmetric supercapacitors on rigid and flexible supports were constructed using an ionic liquid electrolyte with pristine PEDOT, NiS_2 and the PEDOT/NiS_2 hybrid as the electroactive materials. The PEDOT/NiS_2 hybrid based rigid cell delivered a high specific capacitance of 937.5 F g^{-1} compared to 517.5 F g^{-1}, achieved for the PEDOT based cell at the same current density of 10 A g^{-1}. The hybrid also showed excellent cycling stability with ~81% capacitance retention relative to 50.5% capacitance retention at the end of 5000 cycles, obtained for the PEDOT based rigid cell. The energy and power densities achieved for the hybrid cell are: 154.16 W h kg^{-1} and 7.4 kW kg^{-1} respectively, greater by 47 and 4% compared to the PEDOT based cell. The flexible cell based on the PEDOT/NiS_2 hybrid strikingly outperformed the pristine PEDOT or NiS_2 cell, and it exhibited a remarkably large specific capacitance of 1540 F g^{-1} (at 10 A g^{-1}) and showed good cycling stability as well. We also show the applicability of the hybrid as a counter electrode in photoelectrochemical solar cells. The foldability of the flexible cell, the high-rate capability, durability and capacitance of the cell based on the PEDOT/NiS_2 hybrid, and the demonstration of a LED illumination with the same show that this approach of combining PEDOT with NiS_2 can be extended to other redox active metal sulfides as well.

Received 9th October 2015
Accepted 3rd November 2015

DOI: 10.1039/c5ra20917j

www.rsc.org/advances

Introduction

Metal sulfide nanostructures are an emerging class of exciting materials for pseudocapacitor applications due to their high specific power densities, long cycle life, fast charge–discharge rates and low cost.[1,2] Pseudocapacitive materials store energy in the form of charge; they undergo reversible faradaic reactions to store and release charge during operation. While transition metal oxides (RuO_2,[3,4] MnO_2,[5,6] V_2O_5 (ref. 7 and 8) and Co_2O_4 (ref. 9 and 10)) and conjugated polymers (poly(aniline) (PANi),[11,12] poly(pyrrole) (PPy),[13,14] poly(3,4-ethylenedoxythiophene) (PEDOT)[14,15]) have been exhaustively used as electrodes in pseudocapacitors, reports on the application of metal sulfides to supercapacitors are rather sparse. While supercapacitors offer very fast discharge rates and require low maintenance, attaining a high energy density without compromising power density poses a daunting challenge. Energy density of a supercapacitor is given by, $E = 0.5CV^2$, where C is the capacitance and V is voltage window. It can be improved by increasing the output voltage and specific capacitance.[16] To improve the voltage window, ionic liquids and organic liquids are more suitable as electrolytes compared to aqueous media, for the latter incur gas evolution owing to decomposition at high voltages.

Among metal oxides, while RuO_2 (ref. 17 and 18) is recognized as an excellent electrode material due to its high specific capacitance but it is highly expensive. On the contrary, MnO_2 is cheap, offers large specific capacitance and is environmentally benign as well.[19] But metal oxides, by and large, exhibit poor electrical conductivities, and as a consequence, their specific

[a]Department of Chemistry, Indian Institute of Technology Hyderabad, Kandi-502285, Sangareddy, Telangana, India

[b]CSIR-National Physical Laboratory, Dr K. S. Krishnan road, New Delhi-110012, India. E-mail: mdeepa@iith.ac.in; Fax: +91-40-23016003; Tel: +91-40-023016024

† Electronic supplementary information (ESI) available: Cross-sectional image and EDX of the PEDOT–NiS_2 hybrid, XRD patterns of NiS_2 samples obtained at various temperatures, the electrochemical properties of cells based on pristine NiS_2 microspheres, and details of construction of quantum dot solar cells (QDSCs) and characterization. See DOI: 10.1039/c5ra20917j

capacitances are lower than the theoretical values. Further their mixed conduction capability is also dismal, for while metal oxides conduct ions well, they are poor conductors of electrons. Metal chalcogenides (NiS_2,[20,21] CuS,[22,23] CoS,[24,25] $NiCo_2S_4$,[26,27] MoS_2 (ref. 28 and 29)) offer high theoretical capacities, and outstanding electronic, optical and magnetic properties. Among the lot, nickel sulfide is attractive due to the following reasons. It can exist in different stable phases. It can be synthesized in various nanostructured morphologies with great ease and it finds applications in both electrochemical energy storage devices and photovoltaic cells.[30–36] However, the synthesis of nickel sulfide with uniform nanostructured shapes and in pure phase is an arduous task.[37] Some interesting results are summarized here. Zhu *et al.*, reported the synthesis of hierarchical NiS hollow spheres by a hydrothermal route, which delivered a specific capacitance (SC) of 927–583 F g^{-1} at current densities in the range of 4.08–10.2 A g^{-1},[38] in an aqueous alkali based electrolyte. In another report by Chou *et al.*,[36] electrodeposited flaky NiS_2 nanostructures, produced a SC of 717 F g^{-1} at a current density of 2 A g^{-1}, in a 1 M KOH electrolyte. In yet another study, by using a microwave assisted method, NiS_2 nanocubes, nanoparticles and nanospheres were prepared. The NiS_2 nanocubes delivered the highest SC of 695 F g^{-1} at a current density of 1.25 A g^{-1} in a KOH electrolyte solution, due to a faster electron diffusion rate in the cubes compared to the other two structures.[39] In another study, composites of mixed phase NiS–NiS_2 particles decorated over reduced graphene oxide (RGO) were prepared. The composite exhibited a SC of 1000 F g^{-1} at a current density of 10 A g^{-1}, when a Pt wire was used as the counter electrode and an aqueous KOH solution was used as the electrolyte.[40] NiS_2 microspheres with a cubic pyrite structure were prepared by a solvothermal route using an ethylenediamine–glycol mixed solvent, and the phase transformations were studied in detail.[41]

Combining nickel sulfides with RGO nanosheets improves both the capacitance and the cycling stability of the sulfide, for RGO imparts mechanical integrity to the composite and provides a robust highly conductive support for the sulfide particles,[42] which prevents their detachment from the current collector during cycling. In the same vein, conducting polymers have rarely been utilized for enwrapping nickel sulfides, to yield high performance hybrid materials. Conducting polymers offer many advantages. They can be easily switched between reduced (dedoped) and oxidized (doped) states. They are inexpensive, less toxic, and can be easily prepared in bulk or film forms at room temperature. They are highly conducting in their doped states.[43,44] For weight practicability and portability reasons, here, we used carbon (C) fabrics as current collectors. Previously, transparent flexible asymmetric supercapacitors (ASCs) were prepared by coating active materials on In_2O_3 : Sn/poly(ethylene terephthalate) substrates[5] and solid state ASCs were fabricated by coating active materials on carbon cloth.[45] Until now supercapacitors based on PEDOT/NiS_2 hybrids as electroactive materials on rigid or flexible supports have not been studied. The synergistic effects of the two components, the high electrical conductivity of PEDOT in the oxidized state, good chemical stability, impressive redox properties, ease of processing, and the fact that it provides a robust scaffold for the NiS_2 microspheres to anchor to, thus ensuing in a durable pseudocapacitive electrode are clearly reflected in the elaborate performance study presented here.

Here, we present the synthesis of environmentally benign NiS_2 microspheres by a hydrothermal route, followed by electropolymerization of EDOT along with the NiS_2 microspheres, to yield a PEDOT/NiS_2 hybrid, which was deposited on both rigid (stainless steel or SS) and flexible (C-fabric) current collectors. C-fabric was chosen as a substrate due to its cost effectiveness, good electrical conductivity, flexibility and excellent electrochemical stability.[46] The electrochemical charge–discharge characteristics of the PEDOT/NiS_2 hybrid were compared with those of pristine PEDOT and NiS_2 by constructing symmetric cells using C-fabric and SS substrates, and an ionic liquid as the electrolyte. The use of an ionic liquid helps overcome the limitations posed by the conventional aqueous alkaline electrolytes. The superior electrochemical energy storage attributes of the PEDOT/NiS_2 hybrid in the form of a lightweight flexible supercapacitor and the demonstration of a real time application using the same are indicators of the generic applicability of this approach for preparing and using a variety of yet unmapped sulfide/conducting polymer hybrids in high performance energy storage devices.

Experimental

Chemicals

3,4-Ethylenedioxythiophene (EDOT) monomer was purchased from Sigma Aldrich. 1-Butyl-3-methyl imidazolium trifluoromethane sulfonate (BMITFI), nickel chloride hexahydrate ($NiCl_2 \cdot 6H_2O$), sodium thiosulfate pentahydrate ($Na_2S_2O_3 \cdot 5H_2O$), acetone, acetonitrile and ethanol were purchased from Merck chemicals. Ultrapure water (resistivity 18.2 MΩ cm) was obtained through a Millipore direct Q3UV system. A carbon fiber fabric of 3 mm thickness was procured from Alibaba Pvt. Ltd. GF/D borosilicate glass microfiber membrane separators and stainless steel (SS) foils were purchased from Alfa Aesar, and SnO_2:F (FTO) coated glass substrates were purchased from Pilkington. The latter were cleaned with an alkaline soap solution, washed with water, dried and then wiped clean with acetone prior to use.

Synthesis of NiS_2 microspheres and hybrid

$NiCl_2 \cdot 6H_2O$ (2.5 mM) was dissolved in ultrapure water (40 mL). This was followed by the addition of $Na_2S_2O_3 \cdot 5H_2O$ (2.5 mM) at room temperature. The reaction mixture was stirred for 10 min, then transferred into a stainless steel autoclave (of 60 mL capacity) with a polytetrafluoroethylene liner. The autoclave was sealed and heated at 150 °C for 12 h and cooled to room temperature. The reaction mixture was filtered through ashless filter paper (diameter: 750 mm) and washed with a mixture of water and ethanol (1 : 1 v/v ratio), and dried overnight in a vacuum oven at 60 °C. The obtained black colored product was stored in a vacuum desiccator and it is referred to as NiS_2 microspheres. Three more nickel sulfide products were

prepared by following the same procedure, reagent concentrations and heating duration except the heating temperature of the autoclave, which were maintained at 120, 140 and 160 °C separately, to yield a unique product, in each of the three cases.

A clear solution of the monomer, EDOT (0.1 M) was prepared by its' dissolution in the ionic liquid: BMITFI (0.1 M) and acetonitrile (10 mL). A three electrode cell was used for the electrochemical deposition of pristine PEDOT or PEDOT/NiS_2 hybrid films. A stainless steel foil or a carbon fabric or a FTO/glass substrate (area: 1 cm × 2 cm) was employed as the working electrode, a Pt rod was used as the counter electrode and an Ag/AgCl/KCl electrode was used as the reference electrode. Bright blue colored films of PEDOT were obtained by the application of +1.5 V to the working electrode for 600 s, under potentiostatic conditions at room temperature in the chronoamperometric mode. The films were washed in acetonitrile and dried in air. For preparing the hybrid films, to the solution of EDOT (0.1 M) and BMITFI (0.1 M) in acetonitrile, 50 mg of NiS_2 microspheres (product obtained at the end of the 150 °C, 12 h hydrothermal treatment) were added, and the resulting formulation was ultrasonicated for 30 min. The dispersion was employed as the medium in the above-described three electrode cell, and upon application of +1.5 V to the working electrode (SS foil or C-fabric) for 600 s, deep bluish-black colored PEDOT/NiS_2 hybrid films were formed on the working electrode. The films were rinsed in acetonitrile, dried and stored in air. For preparing the NiS_2 electrodes, a slurry of NiS_2 microspheres (0.05 g) was prepared by using NMP (1 mL) as the solvent. This slurry was doctor bladed onto the substrate (C-fabric or SS foil). Upon evaporation of the solvent at room temperature, a black colored dry film of NiS_2 was obtained. The GF/D separators were cut to the size of the active electrodes, wetted with the ionic liquid: BMITFI, and symmetric cells were constructed by carefully placing the wetted separator between two-NiS_2 or PEDOT or PEDOT/NiS_2 hybrid coated SS foils or C-fabrics, the coated surface facing inwards or the separator. A small portion along the edge of the SS foil or the edge of the C-fabric was deliberately left uncoated, and was also not brought in contact with the separator during cell fabrication; electrical contacts were taken from these edges for the measurements. The sides were sealed with an epoxy sealant, and the cells were ready to use.

Instrumental techniques

Galvanostatic charge–discharge curves and electrochemical impedance spectra (EIS) were recorded on an Autolab PGSTAT 302N potentiostat/galvanostat, with a frequency response analyzer and equipped with a NOVA 1.9 software. The surface morphology and microstructure of the pristine NiS_2, pristine PEDOT and PEDOT/NiS_2 hybrid products were studied on a field emission scanning electron microscope (FE-SEM, Carl Zeiss Supra 40) and high resolution transmission electron microscopy (HRTEM) images were acquired on a FEI Tecnai G2 F30 STWIN machine with a FEG source operating at 300 kV. For TEM, a thin layer of the sample was carefully extracted into water, dispersed therein by sonication. The solution as applied to a carbon coated copper grid of 3.05 mm diameter and the solvent was evaporated before use. X-ray diffraction (XRD) was performed to identify the crystal structure of the samples by using a PANalytical, X'pert PRO' with a CuKα (λ = 1.5406 Å) radiation by applying an accelerating voltage of 40 kV and 30 mA current. A Bruker Senterra dispersive micro Raman spectrometer with a laser beam operating at a wavelength of 532 nm was used for recording Raman spectra. Brunauer–Emmett–Teller (BET) specific surface area measurements on the samples was carried out on a Micromeritics, ASAP 2020. Optical absorption spectra of the films were measured on a UV-vis-near infrared (NIR) spectrophotometer (model: Shimadzu UV-3600). Thermogravimetric analysis (TGA) of the electrode materials was performed on a TA Instruments Q600.

Results and discussion

Structural analysis

The XRD patterns of pristine PEDOT, NiS_2 microspheres and the PEDOT/NiS_2 hybrid are shown in Fig. 1a. The structure and bulk phase of the electroactive materials were identified by XRD analysis. NiS_2 microspheres were obtained at the end of the hydrothermal treatment of a nickel chloride and sodium thiosulfate solution at 150 °C for 12 h. The diffractogram of PEDOT shows a very weak peak at $2\theta = 12.2°$ due to the (200) plane of PEDOT. A relatively strong and broad reflection is observed at $2\theta = 26.06°$ which corresponds to an inter-chain stacking of 3.42 Å, and originates from the (020) plane. A similar peak corresponding to the (020) plane of the orthorhombic structure of PEDOT (doped by tosylate ions) was observed in an earlier study.[47] But since the peaks are very broad, PEDOT here is largely amorphous. The XRD pattern of pristine NiS_2 microspheres shows well-resolved intense peaks at d = 3.23, 2.83, 2.53, 2.3, 1.99 and 1.71 Å, and these are attributed to the (111), (200), (210), (211), (220) and (311) planes of the cubic pyrite structure of NiS_2 with lattice parameter, a = 5.67 Å in accordance with the PDF (powder diffraction file) number 030734. The successful conversion of the Ni precursor to NiS_2 is evidenced from the fact that all the observed diffraction peaks

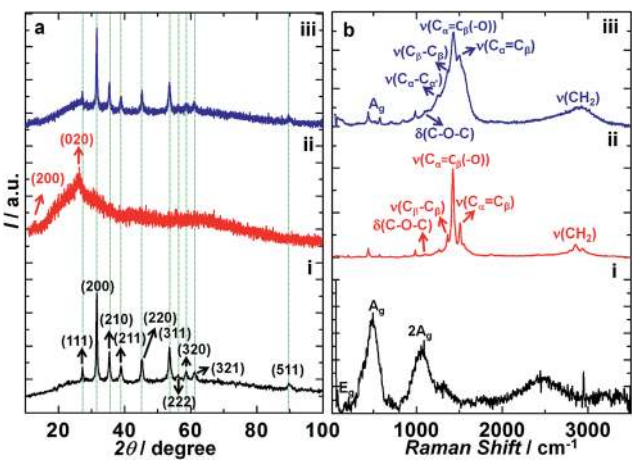

Fig. 1 (a) XRD patterns and (b) Raman spectra of: (i) NiS_2, (ii) PEDOT and (iii) PEDOT/NiS_2 hybrid.

could be assigned to the standard diffraction data of NiS_2, and no impurity phase peaks were detected. The XRD pattern of the PEDOT/NiS_2 hybrid is almost similar to that of pristine NiS_2 with peaks at nearly the same *d* values, with a negligible variation (of the order of ± 0.01 Å in a few *d*-values), in comparison to pristine NiS_2. This suggests that the cubic crystal structure of NiS_2 is preserved in the hybrid. The polymer's peak in the hybrid is overwhelmed by the diffraction pattern of NiS_2, and therefore it could not be identified.

The Raman spectra of pristine PEDOT, NiS_2 microspheres and the EDOT/NiS_2 hybrid recorded in the wavenumber range of 200–2000 cm^{-1} are shown in Fig. 1b. Pristine NiS_2 shows a weak peak at 280 cm^{-1} which is assigned to the E_g phonons followed by two strong peaks at 480 and 1057 cm^{-1} corresponding to A_g phonons and an overtone of the A_g mode, *i.e.*, a combination of $2A_g$ modes of the cubic pyrite NiS_2 crystal respectively. Our assignments agree reasonably well with previously reported Raman scattering data of a plate like single crystal of NiS_2 with a dominant (111) orientation.[48] The 480 cm^{-1} peak, is a composite of two peaks at 480 and 495 cm^{-1}, the latter one is ascribed to T_g phonons.[48] Pristine PEDOT shows a very strong intense peak at 1425 cm^{-1}, corresponding to the symmetric $C_\alpha{=}C_\beta(-O)$ stretching mode, and this peak is flanked by medium intensity peaks on either side; at 1359 cm^{-1} due to the C_β–C_β stretching vibration and at 1511 cm^{-1}, due to the asymmetric $C_\alpha{=}C_\beta$ stretching mode, which align well with the previously reported Raman data of PEDOT.[49] Small peaks/shoulders are also observed at 571, 1098 and 1265 cm^{-1} and these originate from the oxyethylene ring deformation, C–O–C deformation and the C_α–$C_{\alpha'}$ (inter-ring) stretching modes respectively. Medium intensity peaks at 989 and 2851 cm^{-1} are attributed to the oxyethylene ring deformation and the CH_2 stretching modes. The PEDOT/NiS_2 hybrid shows peaks from the polymer which are slightly shifted compared to the pristine polymer. The symmetric $C_\alpha{=}C_\beta(-O)$ and C_β–C_β stretching modes are upshifted to 1434 and 1369 cm^{-1}. The asymmetric $C_\alpha{=}C_\beta$ stretching mode produces a distinct shoulder, which is downshifted by 9 cm^{-1} to 1505 cm^{-1}. Among the peaks due to the Ni–S phonon modes, the A_g phonons' mode is faintly perceptible; and the 2Ag mode at 1057 cm^{-1} is obscured by the preponderance of the δ(C–O–C) mode from PEDOT. The C_α–$C_{\alpha'}$ (inter-ring) stretching frequency also experiences a downshift to 1259 cm^{-1}, in the hybrid. The changes in vibrational frequencies of the polymer in the PEDOT/NiS_2 hybrid are caused by the dipolar interactions between the polar Ni–S bonds and the polar C–S and C–O bonds in the polymer.

The SEM micrographs of pristine NiS_2, pristine PEDOT and the PEDOT/NiS_2 hybrid are shown in Fig. 2. The micrograph of pristine NiS_2 reveals the formation of solid micro-spheres of NiS_2, 2 to 3.5 μm in dimensions, which are well-separated (Fig. 2a). A closer inspection of the spheres (Fig. 2b and c), reveals the spheres to be composed of flattened flakes of NiS_2, but the spheres have distinct grain boundaries. The distribution of spheres is uniform across the sample. The jagged surface of the spheres permits better electrolyte access into the core of the spheres, which can result in improved charge storage capacity. The low magnification image of pristine PEDOT is relatively featureless, with large particles of no particular shape and extending upto a few microns are seen to be distributed randomly (Fig. 2d). The higher magnification images (Fig. 2e and f) show the presence of interlinked irregular shaped particles with no distinguishable grain boundaries. A highly dense network of PEDOT particles is clearly observable in Fig. 2f. The thickness of the PEDOT/NiS_2 hybrid film was found to be 6 μm from the cross-sectional image of the PEDOT/NiS_2 hybrid (ESI, Fig. S1†). The image shows the presence of macro-pores across the cross-section. These are essentially voids between the polymer particles, and therefore the electrolyte can easily seep through the cross-section of the film during electrochemical reactions. The micrograph of the PEDOT/NiS_2 hybrid shows the NiS_2 micro-spheres to be embedded in a layer of PEDOT (Fig. 2g). The spherical shapes which stem from NiS_2 are distinctly visible and they extend over a few tens of microns, indicating the excellent homogeneity of the hybrid material. The average size of the spheres is ~2 μm. It is evident from Fig. 2h and i, that the conducting polymer serves a scaffold over which the NiS_2 micro-spheres are supported, for we observe hemispherical shapes spread uniformly over a wavy sheet of PEDOT and at the same time, the polymer also serves as a shroud which envelopes the spheres. It is also obvious that the structural integrity of the spheres is maintained, after the formation of the hybrid, indicating that PEDOT functions as a conductive interconnect between the otherwise well-segregated NiS_2 spheres. A few lumpy particles of PEDOT are also observed to be superimposed over the NiS_2 microspheres, at some places. After coating of the conductive polymer, the surface of the hybrid is rough compared to pristine sample due to the multi-level growth process of PEDOT polymerization. In the hybrid, the advantages of the two materials intersect, both NiS_2 and PEDOT are highly conducting. PEDOT is a redox polymer, and during charge–discharge, it takes up and releases anions from the electrolyte by undergoing doping–dedoping reactions. Simultaneously, the nanostructured morphology afforded by the NiS_2 microspheres, allows for a greater uptake of anions from the electrolyte during charge–discharge. The synergy between PEDOT and NiS_2 is further reflected in the electrochemical characteristics of the supercapacitors fabricated using the PEDOT/NiS_2 hybrid.

TEM and HRTEM images of NiS_2 microspheres, pristine PEDOT and the PEDOT/NiS_2 hybrid are shown in Fig. 3. Fig. 3a shows the TEM image of NiS_2 microspheres. Solid spherical shapes are distinctly observed, the spheres are discrete, almost 1–2 μm in dimensions with dark contours. The corresponding HRTEM image extracted from the periphery of a microsphere shows crisscross lattice fringes (Fig. 3b). It is observed that the lattice fringes in different regions are oriented along different directions, but these domains are contiguous and overlapping, indicating that the spheres are crystalline. An enlarged view of the lattice fringes is presented in Fig. 3c. The inter-fringe separation is 0.28 nm, which matches well with the inter-layer spacing of 2.83 Å, corresponding to the 200 plane of cubic pyrite NiS_2. A distance of 0.23 nm between adjacent fringes is also identified in Fig. 3b, which agrees with a *d* of 2.3 Å, conforming to the (211) plane of cubic NiS_2. The selected area

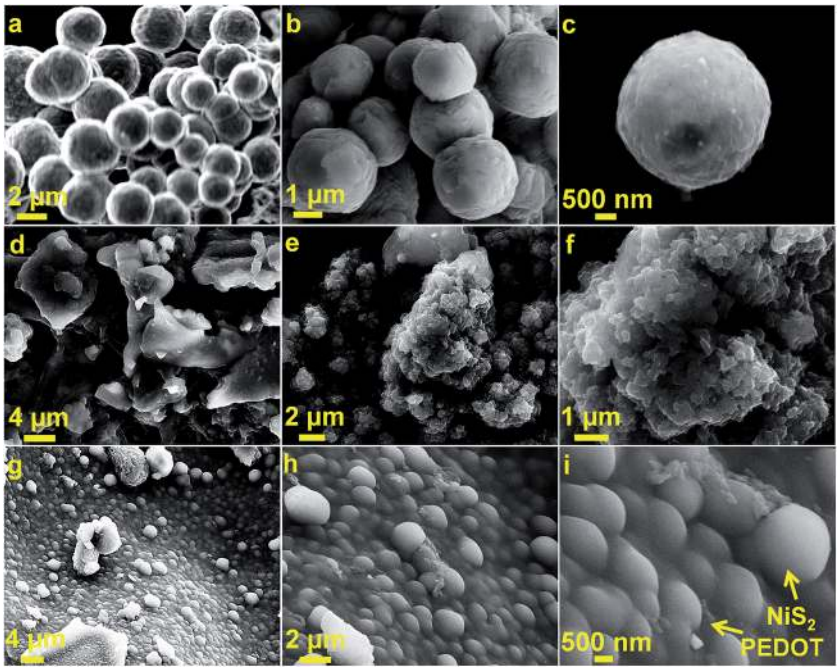

Fig. 2 SEM micrographs of (a–c) NiS_2 microspheres, (d–f) the pristine PEDOT film and (g–i) the PEDOT/NiS_2 hybrid, at different magnifications.

electron diffraction pattern (SAED) of the spheres shows bright spots (Fig. 3d), indicating the good crystalline quality of the NiS_2 spheres. The spots were indexed to the (111) and ($0\bar{2}2$) planes of cubic NiS_2, reaffirming the results obtained from lattice images. The TEM image of pristine PEDOT is displayed in Fig. 3e. The image shows diffused intermingling particles, with no distinct grain-boundaries. A glazy contrast is seen, indicating that the polymer is amorphous. The HRTEM image of the polymer (Fig. 3f) shows some traces of crystallinity, with lattice fringes localized to a very small region. The inter-fringe separation is 0.4 nm, which is close to the inter-chain stacking distance obtained from XRD results of the polymer.

The TEM image of the PEDOT/NiS_2 hybrid (Fig. 3g) shows NiS_2 microspheres coated with a sheath of the polymer (PEDOT). The PEDOT coating serves as a conducting interconnect between the microspheres, and enables superior ion uptake during electrochemical reactions. PEDOT undergoes oxidation and reduction reactions, upon application of an electric voltage or current. Anions are attached to the polymer backbone (doping) during oxidation and they are released back into the electrolyte during reduction (dedoping) and the

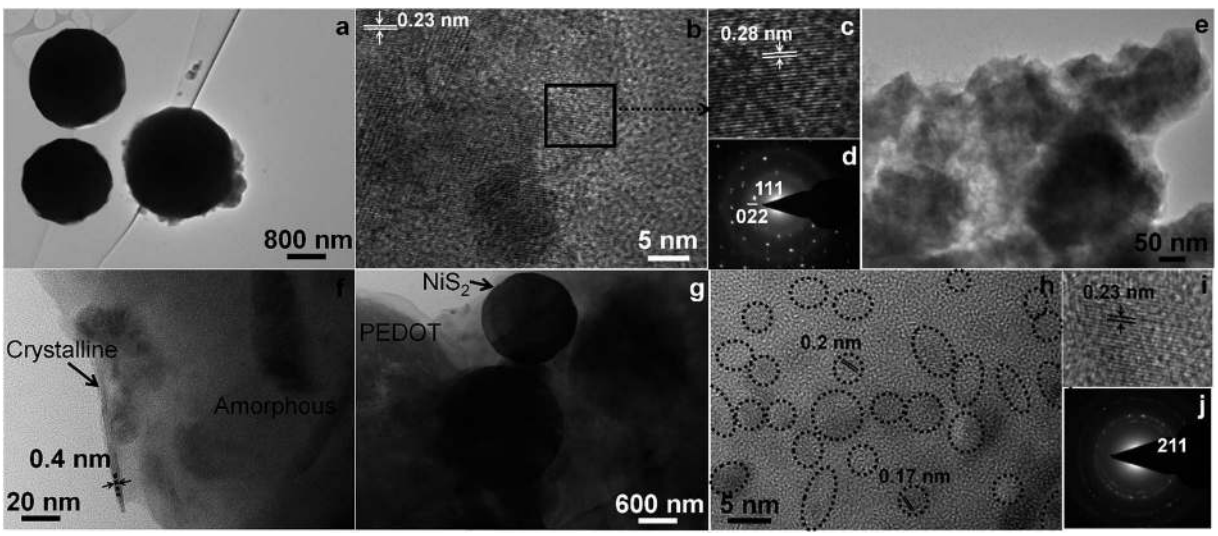

Fig. 3 (a) TEM- and (b and c) HRTEM-images and (d) a SAED pattern of NiS_2 microspheres, (e) TEM- and (f) HRTEM-images of pristine PEDOT, (g) TEM- and (h and i) HRTEM-images and (j) a SAED pattern of the PEDOT/NiS_2 hybrid.

polymer acquires a neutral form. These processes are reversible, and they occur in tandem with the oxidation and reduction of NiS_2. They aid in increasing the net charge storage capacity of the NiS_2 microspheres. A HRTEM image of NiS_2 microspheres in the hybrid is shown in Fig. 3h. The image shows nanocrystallites of NiS_2, approximately 2 to 10 nm in dimensions, but many of them are probably obscured by the overlying polymer. Some of the crystallites have been marked with dotted ellipses/circles in Fig. 3h. Inter-fringe distances of 0.2 and 0.17 nm were identified, which are consistent with *d*-values of 1.99 and 1.7 Å, corresponding to the (220) and (311) planes of cubic NiS_2. However, most of the crystallites show a separation of 0.23 nm; a blown-up view of one such crystallite of NiS_2, is shown in Fig. 3i, which matches with the (211) reflection. Crystallites oriented along different planes prevail in the NiS_2 microspheres, suggestive of the polycrystalline nature of the material. The crystallinity of the NiS_2 microspheres is largely unaffected by the wrapping of the polymer around the spheres. But unlike the pristine microspheres, wherein the fringes are continuous, in the lattice scale image of the hybrid, the domains (of fringes) are separated by amorphous regions, these are due to the polymer (Fig. 3h). The polymer and the NiS_2 microspheres are mixed well in the hybrid. The SAED pattern of the hybrid also differs from that obtained for the pristine microspheres. For the hybrid (Fig. 3j), bright spots superimposed over a diffused ring pattern are observed. The diffuse rings originate from the amorphous polymer, and the spots from the crystalline NiS_2. The SAED pattern, also reaffirms that the polymer and NiS_2 microspheres are juxtaposed or overlapping and therefore have good interfacial contact, which is advantageous for fast charge transfer during electrochemical measurements.

I–V, *I–t* and thermal analysis

The *I–V* characteristics of pristine PEDOT, NiS_2 microspheres and PEDOT/NiS_2 hybrid are shown in Fig. 4a. Pristine PEDOT shows a slight deviation from a linear behavior in the entire applied bias range of −1 to +1 V, indicative of quasi-ohmic dependence of the measured current on the applied bias. The variation of current with voltage is almost linear over a narrow range of potential: −0.25 to +0.25 V (for the PEDOT/NiS_2 hybrid). It is narrower for pristine NiS_2 microspheres, from −0.05 to +0.035 V. Outside of the said potential ranges, the current produced is constant, and is independent of the magnitude of applied bias for both NiS_2 microspheres and the PEDOT/NiS_2 hybrid. From the linear fits restricted to only the ohmic regimes as shown in the figure, the electrical conductivities of the three samples were deduced with the following relation, by using the slope (*I*/*V*), which is the reciprocal of the resistance (R) offered by the sample to electron transport.

$$\sigma\ (\mathrm{mS\ cm^{-1}}) = (I/V)(d/a) = 1/R(d/a) \quad (1)$$

In eqn (1), *d* is the thickness of the electroactive material sandwiched between the two SS plates and *a* is the area of the SS plate in contact with the electroactive material. The conductivities of NiS_2 microspheres, pristine PEDOT and PEDOT/NiS_2 hybrid were calculated to be 1.46, 0.21 and 1.13 mS cm^{-1}. The conductivity of pristine NiS_2 microspheres was highest, and it is closely followed by the conductivity of the hybrid. The conductivity of the PEDOT/NiS_2 hybrid is five-fold times greater than that of PEDOT, and it is comparable to that of NiS_2 microspheres. The synergy between PEDOT and NiS_2 microspheres can be easily gauged from these values, and the profiles of the *I–V* curves. The *I–V* profiles of PEDOT/NiS_2 and NiS_2 are similar but PEDOT shows an altered profile. While for the former two, current saturates at higher values of bias, for pristine PEDOT, there is no current saturation. In the hybrid, besides the structure of the NiS_2 microspheres, the electrical conduction properties of NiS_2 are also preserved despite the fact that the spheres are embedded in PEDOT and coated by PEDOT. While electrical conduction in PEDOT is induced by the polaronic states that are present within the band gap in its' oxidized or doped form, as is the case here, NiS_2 being a narrow band gap semiconductor and possibly due to some defect or trap states within the band gap, shows reasonably high electrical conductivity.

Representative current *versus* time transients corresponding to the formation of PEDOT and PEDOT/NiS_2 hybrid on SS foil from solutions containing EDOT and EDOT along with NiS_2 microspheres respectively are shown in Fig. 4b. When the electrode (SS foil) is swept abruptly from 0 to +1.0 V at $t = 0$ s, a current peak is seen due to electrical double layer capacitive charging, followed by an exponential current decay, and thereafter the current saturates and its' magnitude changes negligibly with time. This trend was common to both solutions (with and without NiS_2 microspheres), albeit the difference in the magnitudes of the initial peak currents. For the solution with and without NiS_2, the i_{peak} values are ~5.6 and ~1.5 mA respectively, indicating that NiS_2 microspheres also diffuse along with the oxidized monomer species to the electrode surface and are responsible for the increased observed current. The formation of PEDOT typically involves the initial oxidation of EDOT, and this oxidized monomer is adsorbed on the electrode surface (SS foil). This is followed by oligomerization, nucleation and growth of the polymer chains on the surface of the electrode. It is apparent that in both cases, the nucleation is almost instantaneous, as the current saturates very rapidly, and this plateau corresponds to polymer chain growth. Since the magnitude of the saturated current is also higher for the film obtained from the solution with NiS_2 microspheres (5.39 mA at $t = 600$ s compared to 0.74 mA for sole PEDOT), it is obvious that the microspheres co-deposit along with the polymer on the electrode surface, and thus the increased currents are explained, (for NiS_2 microspheres are more conducting compared to PEDOT, as judged from *I–V* data analysis). Blue and bluish-black colored films of PEDOT and PEDOT/NiS_2 were obtained at the end of 600 s on SS foils, from solutions without and with NiS_2 microspheres respectively.

The TGA plots for the films of PEDOT and PEDOT/NiS_2 were recorded by scraping off the films from SS foils. These films were deposited on SS foils, by electropolymerization for 600 s in each case. The TGA plots of pristine PEDOT, NiS_2 microspheres, PEDOT/NiS_2 hybrid are shown in Fig. 4c. For NiS_2 microspheres,

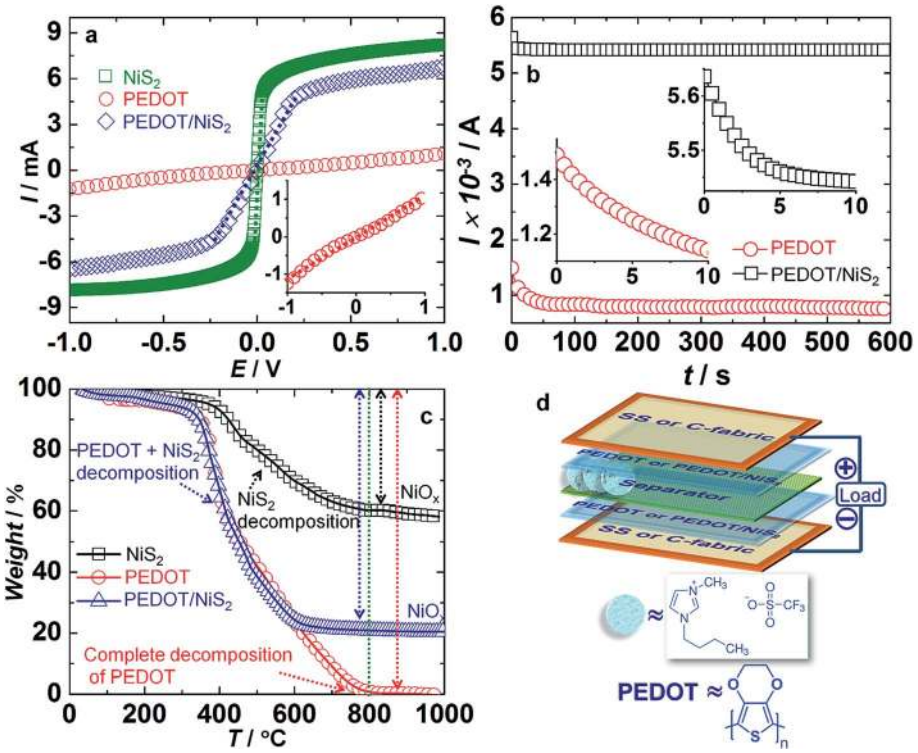

Fig. 4 (a) Linear sweep voltammograms of pristine NiS_2 microspheres (□), neat PEDOT (○) polymer and the PEDOT/NiS_2 (◇) hybrid. NiS_2 microspheres were obtained by heating the precursor in an autoclave at 150 °C for 12 h. (b) Current–time plots recorded during the deposition of PEDOT (○) and PEDOT/NiS_2 hybrid (□) films; insets are magnified views from $t = 0$ to 10 s. (c) TGA plots of NiS_2 (□), PEDOT (○) and PEDOT/NiS_2 hybrid (△) materials. (d) Schematic of the supercapacitor configurations fabricated in this work.

the onset of oxidation to NiO_x is at ~365 °C, and a gradual weight loss continues till 760 °C and thereafter the weight of the remnant material (NiO_x) remains constant till 980 °C. Pristine PEDOT commences to decompose at ~345 °C, and the process continues steadily till it undergoes complete burnout corresponding to a temperature of ~805 °C. The major decomposition of PEDOT/NiS_2 hybrid begins at ~345 °C, and then continues till 606 °C, and subsequently no further weight loss is observed till the end. We used 805 °C as the reference, for at this temperature, PEDOT is completely burnt out whereas NiO_x is left behind for the remaining two samples. The total weight loss experienced by the PEDOT/NiS_2 hybrid is 79.09%, by PEDOT, it is 99.21%, and by NiS_2 39.65%, all at 805 °C. Since the temperature range for oxidation of NiS_2 to NiO_x overlaps with that of decomposition of PEDOT, we find through calculations, that the amount of PEDOT and the proportion of NiS_2 microspheres present in the hybrid are 47.73 and 52.27% respectively. The composition of the hybrid was also determined by energy dispersive X-ray (EDX) analysis (Fig. S2, ESI†). The composition of the hybrid, in terms of elemental atomic percentages is as follows: C: 20%, O: 13%, S: 52% and Ni: 15%. From these values, the amount of NiS_2 present in the hybrid is 49.66%, and PEDOT's proportion is 50.33%, which are close to the values determined by TGA.

The BET surface areas of NiS_2 and PEDOT/NiS_2 were determined to be 8 and 15 $m^2\ g^{-1}$ respectively. The surface area of pristine PEDOT was 2 $m^2\ g^{-1}$. In the past, for NiS_2 microspheres, a surface area of 13.1 $m^2\ g^{-1}$ was reported[50] which compares reasonably well with our value. Here, PEDOT has a very low surface area, but due to the presence of NiS_2 microspheres, the available active surface area for electrochemical reaction is increased and this is also reflected in the electrochemical response.

Growth mechanism

The morphological and structural evolution of NiS_2 microspheres is shown through XRD patterns (Fig. S3, ESI†) and SEM images (Fig. 5), recorded for products obtained by hydrothermally heating of nickel chloride and sodium thiosulfate mixture at four different temperatures of 120, 140, 150 and 160 °C but for the same time span of 12 h. The thiosulfate ions serve as a reductant and also as a structure directing agent. $Na_2S_2O_3 \cdot 5H_2O$ reduces $NiCl_2$ to NiS_2 and oxidizes to Na_2SO_4 according to the following reaction.

$$2Na_2S_2O_3 \cdot 5H_2O + NiCl_2 \rightarrow NiS_2 + Na_2SO_4 + SO_2 + 2NaCl + 5H_2O \quad (2)$$

The XRD patterns of the products obtained at the end of 120 °C hydrothermal treatment shows diffractions peaks corresponding to the cubic pyrite crystalline phase of NiS_2. Peaks corresponding to (200), (210), (211), (220) and (311) planes were clearly observed. A few additional peaks, especially in the 2θ

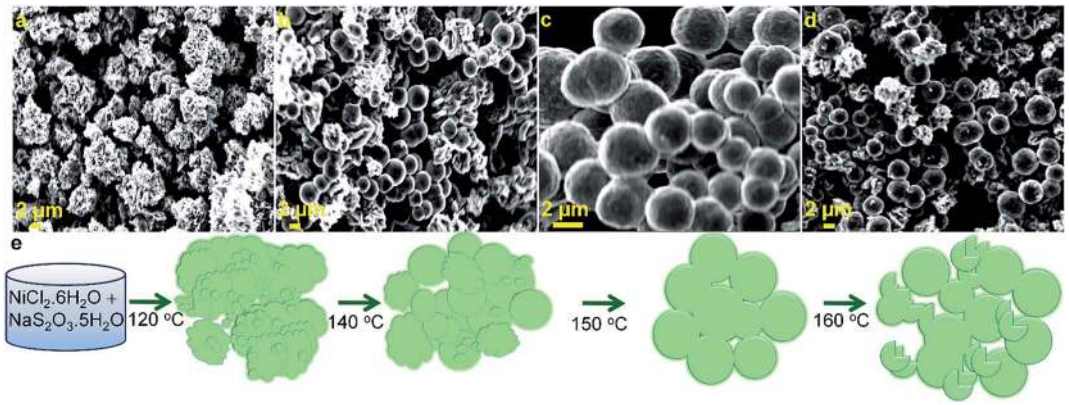

Fig. 5 SEM images of NiS_2 samples, obtained after heating an aqueous solution of 2.5 mM of $NiCl_2 \cdot 6H_2O$ and 2.5 mM $Na_2S_2O_3 \cdot 5H_2O$ at (a) 120 °C, (b) 140 °C, (c) 150 °C and (d) 160 °C for 12 h, under hydrothermal conditions. A schematic of the temperature dependent progressive growth mechanism of NiS_2 is shown in (e).

range of 20 to 30° were also observed (labeled with asterisks), which could not be assigned to any phase of nickel sulfide. These peaks possibly originate from impurities or reaction intermediates, at this juncture. Upon further hydrothermal heating to 140 °C, apart from the peaks due to cubic NiS_2, two extra peaks at $2\theta = 20.4°$ and 26.7° are observed, which again are from intermediates/impurities. Only upon heating at 150 °C or at 160 °C, the pure cubic phase of NiS_2 results. The pattern is devoid of any extraneous peaks. The noticeable difference between XRD patterns of NiS_2 products obtained at the end of 150 and 160 °C hydrothermal treatment, is the increased full width at half maxima values of the principal diffraction peaks for the 160 °C product, indicating a decreased crystallite size at higher temperature. The concomitant micrographs reveal the following: at the end of the 120 °C heating, a particulate morphology is observed, large aggregates of no particular shape and composed of many small particles are formed at this stage. The size of these unshapely aggregates varies from 2 to 8 μm. When the solution was heated at 140 °C, the resulting product shows a mixed morphology comprising of both spheres and aggregated particles. The average diameter of the spheres is about 2 μm. Further heating at 150 °C yields almost monodisperse NiS_2 microspheres, 2 to 3.5 μm in diameter, and no other particles are observed. The microspheres are composed of finer NiS_2 particles. Further heating at an elevated temperature of 160 °C yields randomly distributed ill-defined aggregates in addition to the NiS_2 microspheres, possibly due to the high nucleation rate. When nickel chloride and sodium thiosulfate hydrothermally heated at 120 °C, initially Ni^{2+} species are reduced by $S_2O_3^{2-}$ ions to yield NiS_2 particles and possibly some precipitates of $Ni(OH)_2$ along with other insoluble side products are also formed under the prevailing reducing environment provided by the alkaline medium and at lowered pressure conditions. The latter is probably the reason for the smattering of unassigned XRD peaks in the low 2θ region. The NiS_2 particles tend to aggregate randomly, probably *via* Ostwald ripening to acquire stable structures and a large variance is observed for the aggregate sizes obtained at this point. When the temperature is raised further (140 °C), the larger aggregates are no longer seen. From the peripheries of the aggregates, the particles dissolve back into the liquid (for at higher temperatures under reduced pressure, the products will be more soluble in the liquid) and at the same time, the NiS_2 particles in the core now pack more compactly to form spherical shapes, so as to minimize the solid–liquid interfacial area. At this stage, not all aggregates are converted into spheres. Further heating at 150 °C, induces Ostwald ripening, and the small sized aggregates redissolve in the liquid, and then re-deposit over the NiS_2 microspheres. This is also supported by the increase in the average microsphere size from ~2 to 2.7 μm. This thermodynamically driven spontaneous process occurs because larger particles are more energetically favored than smaller particles. This stems from the fact that molecules on the surface of a particle are energetically less stable than the ones in the interior. Further raising the temperature to 160 °C, again results in a product comprising of NiS_2 microspheres and NiS_2 aggregates. Some of the microspheres break apart due to the available increased thermal energy, they re-dissolve in the solution, and while some re-deposit on the NiS_2 microspheres, the remaining simply crystallize into aggregated NiS_2 particles, which explains the mixed morphology. It must be noted that the NiS_2 obtained at the end of 150 or 160 °C treatment, exists in pure phase, but 150 °C is the optimum temperature, for pure phase microspheres of NiS_2 are formed at this temperature. These findings show that the reaction temperature plays a key role in the formation of NiS_2 microspheres.

Electrochemical characteristics

Symmetric supercapacitor cells were constructed with PEDOT and PEDOT/NiS_2 films on both rigid (SS) and flexible (C-fabric) current collectors. The ionic liquid: 1-butyl-3-methyl imidazolium trifluoromethane sulfonate was employed as the electrolyte. A schematic in Fig. 4d, illustrates the cross-section of rigid or flexible cells. The electrochemical characteristics of the rigid and flexible cells are presented in Fig. 6 and 7 respectively. The CV plots of PEDOT and the PEDOT/NiS_2 hybrid are compared at

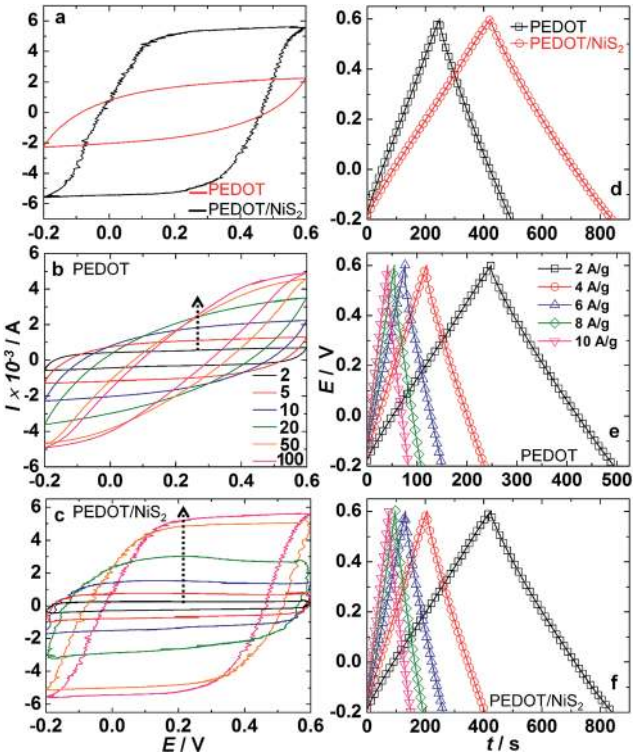

Fig. 6 Comparison of CV plots of (a) PEDOT–PEDOT and PEDOT/NiS_2–PEDOT/NiS_2 based rigid cells recorded at a scan rate of 100 mV s^{-1} and CV plots of (b) PEDOT–PEDOT and (c) PEDOT/NiS_2–PEDOT/NiS_2 based rigid cells recorded at different scan rates of 2, 5, 10, 20, 50 and 100 mV s^{-1}. Comparison of galvanostatic charge–discharge characteristics of (d) PEDOT–PEDOT and PEDOT/NiS_2–PEDOT/NiS_2 cells, at a fixed current density of 10 A g^{-1} and rate capability curves of (e) PEDOT–PEDOT and (f) PEDOT/NiS_2–PEDOT/NiS_2 based cells recorded at 2 (□), 4 (○), 6 (△), 8 (◇) and 10 (▽) A g^{-1}. All cells in (a–f) were symmetric two electrode rigid cells, with SS foils as current collectors.

a scan rate of 100 mV s^{-1} in the voltage window of −0.2 to 0.6 V (Fig. 6a). The CV profile of the PEDOT/NiS_2 hybrid based cell shows a rectangular shape, indicative of the capacitive behavior. The CV curve for the PEDOT based cell has a swollen elliptical shape. Both PEDOT and NiS_2 are pseudocapacitive in nature, for they store and release charge by undergoing oxidation and reduction reactions, as shown in eqn (3) and (4).

$$NiS_2 + x(BuMeIm)^+ + xe^- \rightarrow (BuMeIm)_xNiS_{2-x} \quad (3)$$

$$(PEDOT^+)_x:(TFI)^{x-} + y(TFI)^+ + ye^- \leftrightarrows (PEDOT)_x:(TFI)^{-(x+y)} \quad (4)$$

(Oxidized, pale blue-black) (Reduced, neutral, red)

The area under the CV curve of the PEDOT/NiS_2 hybrid based cell was larger than the area under the curve for PEDOT, at the same scan rate. This implies that the hybrid has a higher ion storage capacity compared to pristine PEDOT. The anodic and cathodic current density maxima of the PEDOT/NiS_2 hybrid based cell are ~3 and ~7 times greater than the current density maxima obtained for the pristine PEDOT based cell. The number of available electroactive sites in the hybrid is much greater than that available on PEDOT. While PEDOT has a granular morphology with closely packed aggregated particles, thus rendering it difficult for the electrolyte ions to access whole of the active material, the hybrid has a textured surface wherein the NiS_2 microspheres embedded in PEDOT are available for reaction with electrolyte ions. The spheres appear as distinct entities which are interconnected by PEDOT, and therefore the ease of electrolyte penetration is high. Furthermore, since the electrical conductivity of the hybrid is also significantly greater than that of the pristine polymer, electron propagation through the hybrid is more facile, and therefore, for every electron injected by the applied bias, during measurement, a charge-compensating cation from the electrolyte is accumulated in the hybrid. The greater ease of ion and electron transport within the hybrid in comparison what is afforded by the pristine polymer is responsible for the observed higher capacitance of the hybrid. The CVs of pristine PEDOT- and PEDOT/NiS_2 hybrid-based cells recorded at different scan rates are displayed in Fig. 6b and c. For both cells, it is observed that the anodic and cathodic current density maxima appear to increase linearly and rapidly as the function of scan rate. For instance, the anodic current density maxima increased from 0.25 to 4.82 mA cm^{-2} (for the PEDOT based cell) and from 0.28 to 5.62 mA cm^{-2} (for the PEDOT/NiS_2 based cell), when the scan rate was raised from 2 to 100 mV s^{-1}. While the shape of the CV curves remained largely elliptical at all scan rates for the pristine PEDOT based cell, the CV shape underwent a noticeable change from oblong (oblate) to (elongated) rectangular for the PEDOT/NiS_2 hybrid based cell from low to high scan rates. Particularly for the PEDOT/NiS_2 hybrid based cell, the CV curves encompass high areas, even at high scan rates. This is suggestive of a good rate capability and reversibility for the PEDOT/NiS_2 hybrid based cell.

Galvanostatic charge–discharge measurements of pristine PEDOT- and the PEDOT/NiS_2 hybrid-based symmetric cells on SS support are shown in Fig. 6d–f. A comparison of charge–discharge curves of pristine PEDOT- *versus* PEDOT/NiS_2 hybrid-based cells, measured at a constant current density of 10 A g^{-1}, over a voltage window of −0.2 to +0.6 V is shown in Fig. 6d. The charge–discharge profiles of the two cells are triangular in shapes and the measured potential during charge–discharge varies linearly with time which is suggestive of the good reversibility of both the materials. The specific capacitances (SC) of the cells were calculated from the slope of discharge curve by using following equation.

$$SC = i \times \Delta t/(\Delta V \times m) \quad (5)$$

In eqn (5), i is the applied current, Δt is the time in seconds for discharge, ΔV is the potential window and m is the mass of the active material assembled on the current collector (serving as working electrode). In the past, Yang *et al.*, reported a SC of 857 F g^{-1} at a current density of 2 A g^{-1} for hierarchical flower shaped β-NiS structures.[51] Another study by Xing *et al.*, reported the preparation of nickel sulfide/reduced graphene oxide, and the composite showed a high SC of 1169 F g^{-1} at 5 A g^{-1}.[40] In

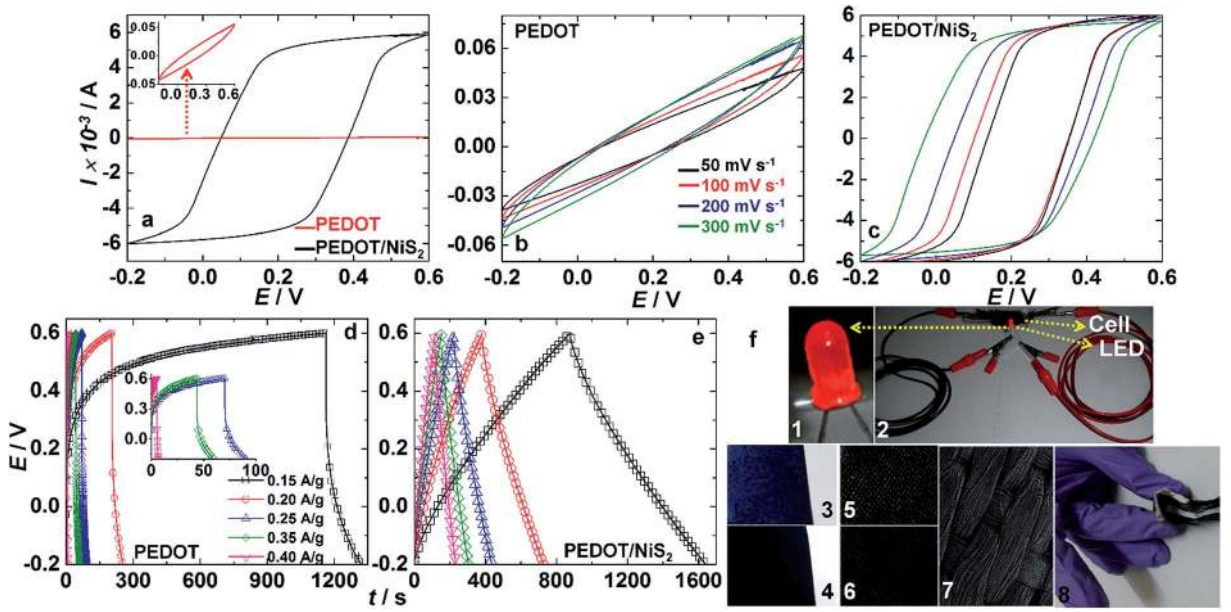

Fig. 7 Comparison of CV plots of (a) PEDOT–PEDOT and PEDOT/NiS_2–PEDOT/NiS_2 flexible supercapacitors recorded at a scan rate of 100 mV s^{-1} and CV plots of (b) PEDOT–PEDOT and (c) PEDOT/NiS_2–PEDOT/NiS_2 based flexible cells recorded at different scan rates of 50, 100, 200 and 300 mV s^{-1}; inset of (a) is an enlarged view of CV of PEDOT. Galvanostatic charge–discharge characteristics of flexible cells of (d) PEDOT–PEDOT, recorded at current densities of 0.15 (□), 0.2 (○), 0.25 (△), 0.35 (◇) and 0.4 (▽) A g^{-1} and (e) PEDOT/NiS_2–PEDOT/NiS_2 recorded at a current densities of 2 (□), 4 (○), 6 (△), 8 (◇) and 10 (▽) A g^{-1}. All cells in (a–e) were symmetric two electrode flexible cells, with C-fabrics as current collectors. (f) (1 and 2) a LED illuminated by a charged C-fabric/PEDOT/NiS_2 based symmetric supercapacitor, (3) a PEDOT film over SS and (4) a PEDOT/NiS_2 film over SS, (5) a blank C-fabric and its' SEM image in (7), (6) a PEDOT/NiS_2 film deposited over C-fabric and (8) the foldability of the C-fabric/PEDOT/NiS_2 based flexible cell.

another report by Xing *et al.*, Ni_3S_2 coated on ZnO array delivered a SC of 1529 F g^{-1} at 2 A g^{-1}.[52] The SC for the PEDOT/NiS_2 based cell, in this study, is ~1041 F g^{-1} (SC = 2 A g^{-1} × 416.4 s/0.79 V) in comparison to the SC of a PEDOT based cell, which is 619.5 F^{-1} (SC = 2 A g^{-1} × 247.8 s/0.78 V) obtained at a current density of 2 A g^{-1}. The huge difference in SC ongoing from the pristine PEDOT based cell to the PEDOT/NiS_2 hybrid based cell is attributed to (a) the large interfacial area between electrode and electrolyte endowed by the NiS_2 microspheres implanted in a sheath of PEDOT, thus increasing the ion uptake capability of the PEDOT/NiS_2 hybrid relative to pristine PEDOT, which does not have a morphology conducive for fast and enhanced ion ingress and egress and (b) the high electrical conductivity of the PEDOT/NiS_2 hybrid, which allows relatively unhindered electron movement within the active material, and this can attract more ions from the electrolyte. At a current density of 2 A g^{-1}, the PEDOT/NiS_2 hybrid exhibits an energy density of 182.6 W h kg^{-1} (416.4/3600 h × 2/0.001 A kg^{-1} × 0.79 V) at a power density of 1.58 kW kg^{-1} (0.79 × 0.001 kV × 2/0.001 A kg^{-1}). Likewise at the same current and power densities, the neat PEDOT polymer delivers an energy density of 107.4 W h kg^{-1} (247.8/3600 h × 2/0.001 A kg^{-1} × 0.78 V).

The rate capabilities of pristine PEDOT- and PEDOT/NiS_2 hybrid-based symmetric cells (fabricated using SS foil current collectors) at different current densities of 2, 4, 6, 8 and 10 A g^{-1} were studied and are shown in Fig. 6e and f respectively. The SC decreased from 619.5 to 517.5 F g^{-1} for the pristine PEDOT based cell and it dropped from 1041 to 937.5 F g^{-1} for the PEDOT/NiS_2 hybrid based cell when the current density was increased from 2 to 10 A g^{-1}. The PEDOT/NiS_2 hybrid based cell exhibits a higher capacitance with better capacitance retention (90% capacitance retention) in comparison to the pristine PEDOT based cell (83.5% capacitance retention) when the current density was raised from 2 to 10 A g^{-1}. The better rate performance of the PEDOT/NiS_2 hybrid reiterates its' usefulness for practical supercapacitors.

The electrochemical responses for the pristine polymer and the hybrid were further evaluated, by using them in lightweight flexible symmetric cells, wherein C-fabrics served as the current collectors. The carbon fiber fabric was characterized by a sheet resistance of 2.7 Ω cm^{-2}, a thickness of ~3 mm and its' weight is 1.8 g cm^{-2}. The PEDOT/NiS_2 hybrid and pristine PEDOT were electropolymerized onto separate C-fabrics. On comparing the CV plots of the pristine PEDOT and PEDOT/NiS_2 hybrid based cells (Fig. 7a, at 100 mV s^{-1}), we again observed that for PEDOT, the CV curve is elliptical whereas for the hybrid, the curve is rectangular. The area under the CV curve for the hybrid based cell is dramatically larger than that under the curve for the pristine PEDOT based cell. This difference is more palpable when we compared the CV plots recorded at different scan rates of 50, 100, 200 and 300 mV s^{-1} for the two cells (Fig. 7b and c). Surprisingly, the area under the CV curves does not increase much with scan rate for the PEDOT based cell, and at all the four scan rates, the curve shape is elliptical. The area under the CV curves increases as a function of scan rate for the PEDOT/NiS_2 hybrid based cell, and the shape of the curve is rectangular

(elongated) almost prolate type, at all the four scan rates. The anodic and cathodic current density maxima are almost two orders of magnitude greater for the PEDOT/NiS_2 hybrid based cell, compared to the counterpart values obtained for the pristine PEDOT based cell. The electrochemical performance differential between the PEDOT/NiS_2 hybrid based cell and the pristine PEDOT based cell is more conspicuous when C-fabrics were used in comparison to the differential achieved with SS foils. Perhaps the pristine polymer does not tether well with the C-fabric, whereas the PEDOT/NiS_2 hybrid does. The poor current densities shown by the PEDOT based cell during CV studies are possibly because of this reason.

The galvanostatic charge–discharge curves of pristine PEDOT- and the PEDOT/NiS_2 hybrid-based flexible symmetric cells at the different current densities are shown in Fig. 7d and e. The photographs of SS foils coated with PEDOT and PEDOT/NiS_2 hybrid, the hybrid coated over C-fabric are shown in Fig. 7f. The PEDOT based cell did not yield any response, when it was charged/discharged at high current densities. Therefore the current densities employed for charging/discharging the PEDOT based cell between the voltage window of −0.2 to +0.6 V were fixed in the range of 0.15 to 0.40 A g^{-1}. The PEDOT/NiS_2 hybrid based cell however could be charged/discharged at high current densities, and therefore the rate capability of this cell was measured at 2, 4, 6, 8 and 10 A g^{-1} (similar to the current densities used for the cells constructed with SS foils). The charge/discharge profile for the pristine PEDOT based flexible cell was no longer triangular, as it was in the case of rigid cells on SS foils. We observed a long-drawn out arc characteristic of a slow charging profile, followed by an abrupt and fast discharge, at any given current density. A large difference was observed between charging- and discharging-times, which is not an indicator of an ideal supercapacitor. As an illustrative example, at 0.15 A g^{-1}, for the PEDOT based flexible cell, the charging time is ∼1162 s, and the cell is discharged in ∼158 s. In contrast, the PEDOT/NiS_2 hybrid based flexible cell retained the triangular charge/discharge profiles at all current densities, with little difference between charge- and discharge-times, at any given current density. The SC for the PEDOT/NiS_2 hybrid based flexible cell drops from 1906 to 1440 F g^{-1}, when the current density was increased from 2 to 10 A g^{-1}. For the pristine PEDOT based flexible cell, it decreases from ∼158 to 1.4 F g^{-1} when the current density is increased from 0.15 to 0.4 A g^{-1}. The SC observed for the PEDOT/NiS_2 hybrid based flexible cell at 10 A g^{-1}. It is slightly higher than the value attained at the same current density for the corresponding rigid cell (937.5 F g^{-1}). The fibrillar network of the C-fabric, allows for better adsorption of the PEDOT/NiS_2 hybrid, leading to an improved interfacial quality for the hybrid/C-fabric compared to hybrid/SS. The capacitance retention for the PEDOT/NiS_2 hybrid based flexible cell is only 75.5% (over the 2 to 10 A g^{-1} span) which is considerably lower than a value of 90%, achieved for the corresponding rigid cell, over the same current density span. The PEDOT/NiS_2 hybrid based flexible cell shows a higher capacitance than the corresponding rigid cell at 2 A g^{-1}, but the converse is true at a higher current density of 10 A g^{-1}. It is inferred that the undulating fibrillar morphology of the C-fabric allows for better ion uptake when the applied current density is low, but is not equally efficient at higher current densities. On the other hand, the smooth, planar surface of the SS foil is equally effective at both high and low current densities. Perhaps some surface treatment is required for the C-fabric which can improve its' performance at high current densities, and this will be done in future. The illumination of a LED with a charged PEDOT/NiS_2 hybrid based flexible symmetric cell is shown in Fig. 7f. The distensibility of the cell is also shown therein, even upon folding it by almost 180°, the cell remains intact; we did not observe any performance difference upon folding the cell. These factors bring out the potential of this PEDOT/NiS_2 hybrid film tethered to C-fabric for practical applications.

In the past, Zhu *et al.*,[53] reported 1D hierarchical structures of a CNT@Ni_3S_2 composite with a SC of 480 F g^{-1} at a current density of 5.3 A g^{-1}. In another report by Zhang *et al.*,[54] bacteria assisted RGO/Ni_3S_2 (BGNS) networks were developed, and the SC was 1424 F g^{-1} at 0.75 A g^{-1}. In yet another report by Wang *et al.*,[55] for a NiS/GO nanocomposite, a SC of 800 F g^{-1} was observed at 1 A g^{-1}. Recently, Zhou *et al.*, synthesized $Ni(OH)_2$ nanosheets coated on single crystal Ni_3S_2 nanorods grown onto the surface of 3D graphene networks (Ni_3S_2@$Ni(OH)_2$/3DGN) and found the SC to be 1037.5 F g^{-1} at 5.1 A g^{-1}.[56] Our results are higher or comparable to literature values on nickel sulfide based composites with carbon nanostructures.

The long term cycling stabilities of pristine PEDOT- and PEDOT/NiS_2 hybrid-based rigid symmetric cells (with films on SS foils as current collectors) were studied by repeating the charge–discharge processes at a current density of 10 A g^{-1} over 5000 cycles and the SC values *versus* cycle number are shown in Fig. 8a. The inset of Fig. 8a shows the cyclability of the flexible symmetric supercapacitor based on the PEDOT/NiS_2 hybrid at the same current density of 10 A g^{-1} over 1000 cycles. The PEDOT/NiS_2 hybrid based cell exhibits a higher SC value and excellent cycling stability compared to the pristine PEDOT based cell. The PEDOT/NiS_2 hybrid- and pristine PEDOT-cells show ∼81% (760 F g^{-1}) and ∼51% (262 F g^{-1}) capacity retention after 5000 cycles respectively. The flexible supercapacitor (with the PEDOT/NiS_2 hybrid) exhibits 80% capacitance retention after 1000 cycles. The superior cycling stability of the hybrid is due to the robust microstructure provided by NiS_2 microspheres which prevent PEDOT from detaching from the current collector's surface and *vice versa*. The NiS_2 microspheres maintain the mechanical integrity of the active material and inhibit the conducting polymer, PEDOT from swelling and shrinking during long term repeated charge–discharge. This microstructural advantage is not available to the cell based on pristine PEDOT, and therefore it experiences a more severe capacitance fading as a function of cycling.

Symmetric cells were also constructed in the NiS_2–NiS_2 configuration with an IL electrolyte soaked separator affixed between the two layers. However, unlike the PEDOT or PEDOT/NiS_2 coatings which were electrodeposited on the current collectors, the NiS_2 coating was deposited by doctor blading. The electrochemical characteristics (cyclic voltammograms (CV) and charge–discharge data, and cycling stability) of the cells are shown in Fig. S4 (ESI†). However, the performance of the

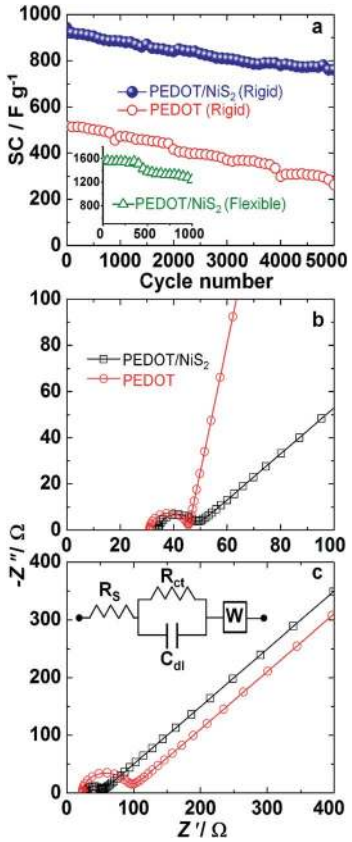

Fig. 8 (a) Specific capacitance variation as a function of number of charge–discharge cycles recorded at a current density of 10 A g^{-1}, for the symmetric PEDOT/NiS_2–PEDOT/NiS_2 (□) and PEDOT–PEDOT (○) rigid cells (supported on SS foils). Nyquist plots of symmetric PEDOT/NiS_2–PEDOT/NiS_2 (□) and PEDOT–PEDOT (○) rigid cells: (b) before cycling and (c) after 5000 cycles, in the frequency range of 0.01 Hz to 1 M Hz. Inset of (a) shows the cycling response of the PEDOT/NiS_2–PEDOT/NiS_2 flexible cell, supported on C-fabrics at a current density of 10 A g^{-1}.

pristine NiS_2 based cells was abysmal, due to the poor adhesion of NiS_2 with the current collectors (be it SS foil or the C-fabric). When NiS_2 is used in combination with PEDOT, the performance improved, due to the synergy between the two components. PEDOT is an elastomeric polymer, which adheres well to the current collector. It also acts as a conductive glues which binds the microspheres, and envelopes them effectively, during electropolymerization.

Nyquist plots of the pristine PEDOT- and PEDOT/NiS_2 hybrid-based rigid symmetric cells, prior to cycling and after 5000 cycles, under an ac perturbation of 0.5 mV, in the frequency range of 0.01 Hz to 1 M Hz are shown in Fig. 8b and c and the corresponding manually calculated parameters are summarized in Table 1. Almost all the plots are composed of a semicircle in the high to medium frequency region followed by an inclined straight line in low frequency region. The semicircle arises from a parallel combination of interfacial resistance or charge transfer resistance at the electrode/electrolyte interface and an electrical double layer capacitance. The sloping line represents a diffusion controlled process. The high

Table 1 EIS parameters corresponding to the experimental data plotted in Fig. 8b and c

Material	Y_o (Ω^{-1} $s^{-1/2}$)	C (μF)	R_{ct} (Ω)	R_s (Ω)
Before cycling				
PEDOT/NiS_2	0.009	3.5023	15.2	32.2
PEDOT	0.0078	549	16.7	29.7
After 5000 cycles				
PEDOT/NiS_2	0.0098	3.57	31	25.4
PEDOT	0.0058	0.350	93.7	18.7

frequency intercept on the real axis is assigned to the contact and electrolyte resistances. The width of the arc is shorter for the hybrid (PEDOT/NiS_2), compared to the pristine polymer (PEDOT). This indicates that the charge transfer resistance at the electrolyte/hybrid interface is smaller than that at the electrolyte/polymer interface and the redox system is kinetically fast. After 5000 cycles, the charge transfer resistance increased from 15.2 to 31 Ω and from 16.7 to 93.7 Ω for the PEDOT/NiS_2- and PEDOT-based cells respectively. The triflate anion transfer at the electrolyte/hybrid interface and electron transfer at the FTO/hybrid interface are faster than the corresponding rates in the pristine polymer. The increase in R_{ct} values with cycling is linked to polymer swelling and shrinking upon repeated ion insertion and extraction process, which causes the pulverization of active material from current collector into the electrolyte. The movement of ion through the bulk of the electrode materials (PEDOT/NiS_2 and PEDOT) is also reflected in the magnitude of Y_o, the Warburg parameter. Y_o was 1.15 times (before cycling) greater for the PEDOT/NiS_2 hybrid relative to PEDOT, which indicates that the NiS_2 microspheres provide facile pathways for ion and electron movement in the PEDOT/NiS_2 hybrid.

Electro-optical properties

PEDOT being an electrochromic polymer, can undergo a reversible change in its' optical properties, upon application of an electric voltage or current.[57] The electro-optical spectra of pristine PEDOT and PEDOT/NiS_2 (films deposited over FTO coated glass substrates) in oxidized and reduced forms in the visible region of the solar spectrum are shown in Fig. 9a. In the oxidized form or doped state, PEDOT is pale blue colored and this state is optically transparent.[58] The flat absorption profiles observed for both pristine PEDOT and the PEDOT/NiS_2 hybrid in the visible range are proofs for the high transmission of the blue state of the polymer. A broad absorption peak is observed in the near infrared region for both films, and this arises from the bipolaronic transitions in PEDOT. Upon reduction by application of −1.5 V to the PEDOT film or the PEDOT/NiS_2 film in a solution of 0.1 M KOH, with a Pt rod as the counter electrode, the films turn deep blue, corresponding to the formation of the neutral polymer. The absorption spectra of the reduced films, now show a strong peak with a λ_{max} at 621 nm (for PEDOT) due to π–π* transitions in the polymer. The peak experiences a bathochromic shift in the hybrid with a λ_{max} at

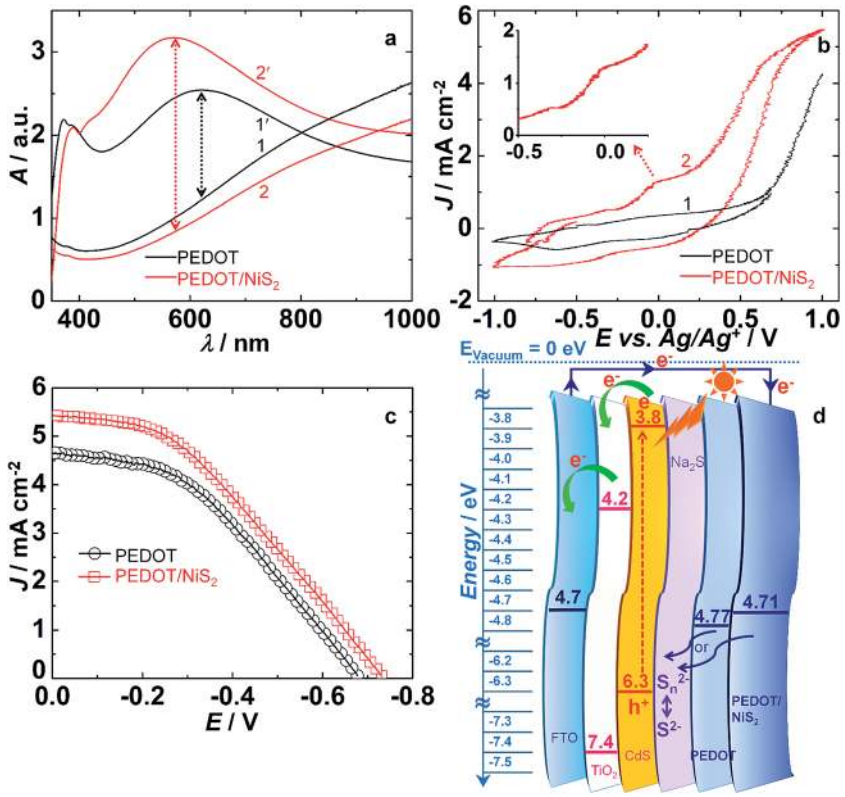

Fig. 9 (a) Absorption spectra of PEDOT and PEDOT/NiS_2 hybrid films on FTO/glass substrates in oxidized (1, 2) and reduced (1′, 2′) states, (b) CV plots of PEDOT (1) and PEDOT/NiS_2 hybrid (2) films recorded at a low scan rate of 10 mV s^{-1} in a 0.1 M KOH solution, (c) *J*–*V* characteristics of photoelectrochemical solar cells with PEDOT (○) and PEDOT/NiS_2 hybrid (□) films as counter electrodes, recorded under 1 sun irradiance (100 mW cm^{-2}), with a CdS/TiO_2 film on FTO/glass as the photoanode a 0.1 M Na_2S solution as electrolyte and (d) energetics and photogenerated electron flow direction in the solar cell.

570 nm. For the same value of applied voltage, the magnitude of absorption contrast, is higher for the PEDOT/NiS_2 hybrid (ΔA = 2.3 a.u. at λ_{max}) compared to the pristine PEDOT film (ΔA = 1.3 a.u. at λ_{max}). The increased ion storage capacity of the hybrid induced by the NiS_2 microspheres is responsible for the enhanced optical contrast obtained for the hybrid. Our results agree very well with previously reported spectra of PEDOT films.[57]

Since PEDOT is electrically conductive and has a work function in the range of 4.7–5.0 eV (depending upon the dopant type), it is most suitable for use as a counter electrode in photoelectrochemical solar cells.[59] To determine the work function of PEDOT and the PEDOT/NiS_2 films, CV plots were recorded for the films in an aqueous solution of 0.1 M KOH with Ag/AgCl/KCl as the reference and a Pt rod as the counter electrode (Fig. 9b). For the hybrid, an oxidation peak was observed in the anodic sweep at +0.01 V *versus* Ag/AgCl/KCl, and this E_{ox} can be equated to the valence band (VB) position of the PEDOT/NiS_2 hybrid. So, E_{ox} (*versus* normal hydrogen electrode (NHE)) of the PEDOT/NiS_2 hybrid = +0.01 V + 0.197 V = +0.207 V. The value of +0.207 V (*versus* NHE) in eV is given by: −4.5 eV − (+0.207 V) = −4.707 ≅ −4.71 eV. Similarly, the E_{ox} for PEDOT is +0.07 V, and by a similar calculation, the VB position for PEDOT is −4.767 ≅ −4.77 eV. The VB position is equivalent to the work function of PEDOT, and we find that the work function of the hybrid is shallower than that of pristine PEDOT. A shallower work-function and the higher electrical conductivity of the hybrid compared to PEDOT is more useful for application in a photoelectrochemical solar cell. Photoelectrochemical solar cells were assembled using cadmium sulfide quantum dots sensitized TiO_2 electrode as the photoanode, a 0.1 M Na_2S solution as the electrolyte and PEDOT or PEDOT/NiS_2 hybrid films (over FTO) as the counter electrode. Detailed procedure on solar cell construction and characterization are provided in the ESI.† The *J*–*V* (current density *versus* applied bias) characteristics under 1 sun (100 mW cm^{-2}) illumination for the photoelectrochemical cells with PEDOT or PEDOT/NiS_2 hybrid films are displayed in Fig. 9c.

When sunlight falls upon the cell, the following processes occur spontaneously, for these are thermodynamically favorable phenomena. (i) Electrons are excited from the VB of CdS to the CB of CdS, and from the CB of CdS, they cascade into the CB of TiO_2, and then to FTO. (ii) Through the external circuit, the electrons reach the counter electrode (PEDOT or PEDOT/NiS_2 hybrid), and they are used up for the reduction of the sulfide species. Greater the catalytic activity of the counter electrode, and higher the electronic conductivity, more efficient would be the sulfide radical reduction, and therefore the PEDOT/NiS_2 hybrid shows a superior performance compared to the pristine polymer. (iii) The reduced sulfide now diffuses to the

photoanode (CdS/TiO_2). It undergoes oxidation, and replenishes the hole in CdS, thus regenerating the anode. In this way, the cell produces photocurrent. These light activated processes and the energetics of the cell can be easily understood from a schematic in Fig. 9d. The performance metrics for the cell with the PEDOT/NiS_2 hybrid (Table S1†) are: open circuit voltage or $V_{OC} = 734$ mV, short circuit current density or $J_{SC} = 5.42$ mA cm^{-2}, fill factor or FF = 37.91, and power conversion efficiency (PCE) or $\eta = 1.51\%$. For the cell with PEDOT, the values are: $V_{OC} = 680$ mV, $J_{SC} = 4.65$ mA cm^{-2}, FF = 40.84, and PCE = 1.29%. The efficiency of the cell with the hybrid is ~17% greater than that of the cell with PEDOT, clearly demonstrating that the PEDOT/NiS_2 hybrid can be used in energy harvesting applications as well.

Conclusions

The outstanding reversible faradaic charge storage characteristics of NiS_2 microspheres embedded in a sheath of the conducting polymer, PEDOT originate from the synergy between the two redox active moieties. NiS_2 microspheres are electronically conducting, have a large surface area, for they are made up of flaky nanoparticles of NiS_2, and thus allow deep electrolyte permeation, which allows increased ion uptake. PEDOT serves as a resilient, stable, conducting glue, to which the NiS_2 microspheres bind and are inhibited from aggregation. The electrochemical performance comparison of symmetric supercapacitors rendered on rigid SS foils and flexible C-fabric current collectors, by using pristine PEDOT, NiS_2 and the PEDOT/NiS_2 hybrid as the electroactive layers revealed the advantage of the synergizing effects of PEDOT and NiS_2 in the hybrid. The performance metrics of the PEDOT/NiS_2 hybrid based rigid cell are: SC 937.5 F g^{-1} (at 10 A g^{-1}) and energy density of 154.2 W h kg^{-1} at a power density of 7.4 kW kg^{-1}, and thus the hybrid surpasses the pristine polymer and sulfide by a huge margin. The superior rate capability and long term cycling stability with ~81% capacitance retention at the end of 5000 cycles achieved for the hybrid based cell clearly indicate that the microstructure of the hybrid and the interfacial structure at the hybrid electrode/electrolyte contact are more conducive for fast, reversible and enhanced charge insertion, relative to the pristine PEDOT or NiS_2 based cells. The hybrid is also useful as a counter electrode in photoelectrochemical solar cells. The demonstration of the first-rate electrochemical behavior of the flexible, bendable cell based on the PEDOT/NiS_2 hybrid (SC ~1440 F g^{-1} (at 10 A g^{-1}) and a capacitance retention of 80% at the end of 1000 cycles), coupled with the lighting up of a LED using the same, are pointers for the promise this method of combining conducting polymers with metal sulfide nanostructures holds for rendering practical cells for real time applications.

Acknowledgements

Financial support from Department of Science and Technology (DST/TM/SERI/2K12-11(G)) is gratefully acknowledged. One of us (RM) also thanks the University Grants Commission (UGC) for SRF.

References

1 W. Wei, L. Mi, Y. Gao, Z. Zheng, W. Chen and X. Guan, *Chem. Mater.*, 2014, **26**, 3418–3426.
2 X. Xia, C. Zhu, J. Luo, Z. Zeng, C. Guan, C. F. Ng, H. Zhang and H. J. Fan, *Small*, 2014, **10**, 766–773.
3 R. Liu, J. Duay, T. Lane and S. B. Lee, *Phys. Chem. Chem. Phys.*, 2010, **12**, 4309–4316.
4 V. Subramanian, S. C. Hall, P. H. Smith and B. Rambabu, *Solid State Ionics*, 2004, **175**, 511–515.
5 R. Liu and S. B. Lee, *J. Am. Chem. Soc.*, 2008, **130**, 2942–2943.
6 Z. Fan, J. Yan, T. Wei, L. Zhi, G. Ning, T. Li and F. Wei, *Adv. Funct. Mater.*, 2011, **21**, 2366–2375.
7 B. N. Reddy, R. Mukkabla, M. Deepa and P. Ghosal, *RSC Adv.*, 2015, **5**, 31422–31433.
8 Q. Qu, Y. Zhu, X. Gao and Y. Wu, *Adv. Energy Mater.*, 2012, **2**, 950–955.
9 R. B. Rakhi, W. Chen, D. Cha and H. N. Alshareef, *Nano Lett.*, 2012, **12**, 2559–2567.
10 Z. J. Yu, Y. Dai and W. Chen, *Adv. Mater. Res.*, 2009, **66**, 280–283.
11 H. Mi, X. Zhang, S. Yang, X. Ye and J. Luo, *Mater. Chem. Phys.*, 2008, **112**, 127–131.
12 H. Wang, Q. Hao, X. Yang, L. Lu and X. Wang, *Nanoscale*, 2010, **2**, 2164–2170.
13 D. Zhang, X. Zhang, Y. Chen, P. Yu, C. Wang and Y. Ma, *J. Power Sources*, 2011, **196**, 5990–5996.
14 J. Wang, Y. Xu, X. Chen and X. Du, *J. Power Sources*, 2007, **163**, 1120–1125.
15 K. S. Ryu, Y. G. Lee, Y. S. Hong, Y. J. Park, X. Wu, K. M. Kim, M. G. Kang, N. G. Park and S. H. Chang, *Electrochim. Acta*, 2004, **50**, 843–847.
16 P. C. Chen, G. Shen, Y. Shi, H. Chen and C. Zhou, *ACS Nano*, 2013, **4**, 178–182.
17 C. C. Hu, K. H. Chang, M. C. Lin and Y. T. Wu, *Nano Lett.*, 2006, **6**, 2690–2695.
18 K. Kuratani, H. Tanaka, T. Takeuchi, N. Takeichi, T. Kiyobayashi and N. Kuriyama, *J. Power Sources*, 2009, **191**, 684–687.
19 X. Lu, T. Zhai, X. Zhang, Y. Shen, L. Yuan, B. Hu, L. Gong, J. Chen, Y. Gao, J. Zhou, Y. Tong and Z. L. Wang, *Adv. Mater.*, 2012, **24**, 938–944.
20 X. Li, J. Shen, N. Li and M. Ye, *Mater. Lett.*, 2015, **139**, 81–85.
21 C. S. Dai, P. Y. Chien, J. Y. Lin, S. W. Chou, W. K. Wu, P. H. Li, K. Y. Wu and T. W. Lin, *ACS Appl. Mater. Interfaces*, 2013, **5**, 12168–12174.
22 K. J. Huang, J. Z. Zhang and Y. Fan, *J. Alloys Compd.*, 2015, **625**, 158–163.
23 T. Zhu, B. Xia, L. Zhou and X. W. D. Lou, *J. Mater. Chem.*, 2012, **22**, 7851–7855.
24 F. Tao, Y. Q. Zhao, G. Q. Zhang and H. L. Li, *Electrochem. Commun.*, 2007, **9**, 1282–1287.
25 S. J. Bao, C. M. Li, C. X. Guo and Y. Qiao, *J. Power Sources*, 2008, **180**, 676–681.

26 H. Wan, J. Jiang, J. Yu, K. Xu, L. Miao, L. Zhang, H. Chen and Y. Ruan, *Cryst. Eng. Comm.*, 2013, **15**, 7649–7651.
27 S. Peng, L. Li, C. Li, H. Tan, R. Cai, H. Yu, S. Mhaisalkar, M. Srinivasan, S. Ramakrishna and Q. Yan, *Chem. Commun.*, 2013, **49**, 10178–10180.
28 J. Soon and K. P. Loh, *Electrochem. Solid-State Lett.*, 2007, **10**, A250–A254.
29 G. Ma, H. Peng, J. Mu, H. Huang, X. Zhou and Z. Lei, *J. Power Sources*, 2013, **229**, 72–78.
30 R. D. Apostolova, O. V. Kolomoyets, Y. A. Tkachenko and E. M. Shembel, *Russ. J. Appl. Chem.*, 2012, **85**, 612–615.
31 Q. Pan, J. Xie, S. Liu, G. Cao, T. Zhu and X. Zhao, *RSC Adv.*, 2013, **3**, 3899–3906.
32 S. Ni, X. Yang and T. Li, *J. Mater. Chem.*, 2012, **22**, 2395–2397.
33 Y. Wang, Q. Zhu, L. Tao and X. Su, *J. Mater. Chem.*, 2011, **21**, 9248–9254.
34 H. Sun, D. Qin, S. Huang, X. Guo, D. Li, Y. Luo and Q. Meng, *Energy Environ. Sci.*, 2011, **4**, 2630–2637.
35 W. M. Kriven, *J. Am. Ceram. Soc.*, 1988, **71**, 1021–1030.
36 S. W. Chou and J. Y. Lin, *J. Electrochem. Soc.*, 2013, **160**, 178–182.
37 L. Zhang, J. C. Yu, M. Mo, L. Wu, Q. Li and K. W. Kwong, *J. Am. Chem. Soc.*, 2004, **126**, 8116–8117.
38 B. T. Zhu, Z. Wang, S. Ding, J. S. Chen and X. W. D. Lou, *RSC Adv.*, 2011, **1**, 397–400.
39 H. Pang, C. Wei, X. Li, G. Li, Y. Ma, S. Li, J. Chen and J. Zhang, *Sci. Rep.*, 2014, **4**, 1–8.
40 Z. Xing, Q. Chu, X. Ren, J. Tian, A. M. Asiri, K. A. Alamry, A. O. Al-Youbi and X. Sun, *Electrochem. Commun.*, 2013, **32**, 9–13.
41 S. L. Yang, H. B. Yao, M. R. Gao and S. H. Yu, *CrystEngComm*, 2009, **11**, 1383–1390.
42 J. Yang, X. Duan, W. Guo, D. Li, H. Zhang and W. Zheng, *Nano Energy*, 2014, **5**, 74–81.
43 G. Wang, L. Zhang and J. Zhang, *Chem. Soc. Rev.*, 2012, **41**, 797–828.
44 G. A. Snook, P. Kao and A. S. Best, *J. Power Sources*, 2011, **196**, 1–12.
45 X. Lu, M. Yu, G. Wang, T. Zhai, S. Xie, Y. Ling, Y. Tong and Y. Li, *Adv. Mater.*, 2013, **25**, 267–272.
46 Y. C. Chen, Y. K. Hsu, Y. G. Lin, Y. K. Lin, Y. Y. Horng, L. C. Chen and K. H. Chen, *Electrochim. Acta*, 2011, **56**, 7124–7130.
47 T. Y. Kim, C. M. Park, J. E. Kim and K. S. Suh, *Synth. Met.*, 2005, **149**, 169–174.
48 T. Suzuki, K. Uchinokura, T. Sekine and E. Matsuura, *Solid State Commun.*, 1977, **23**, 847–852.
49 S. Garreau, G. Louarn, J. P. Buisson, G. Froyer and S. Lefrant, *Macromolecules*, 1999, **32**, 6807–6812.
50 Z. Wan, C. Jia and Y. Wang, *Nanoscale*, 2015, **7**, 12737–12742.
51 J. Yang, X. Duan, Q. Qin and W. Zheng, *J. Mater. Chem. A*, 2013, **1**, 7880–7884.
52 Z. Xing, Q. Chu, X. Ren, C. Ge, A. H. Qusti, A. M. Asiri and X. Sun, *J. Power Sources*, 2014, **245**, 463–467.
53 T. Zhu, H. B. Wu, Y. Wang, R. Xu and X. W. Lou, *Adv. Eng. Mater.*, 2012, **2**, 1497–1502.
54 H. Zhang, X. Yu, D. Guo, B. Qu, M. Zhang, Q. Li and T. Wang, *ACS Appl. Mater. Interfaces*, 2013, **5**, 7335–7340.
55 A. Wang, H. Wang, S. Zhang, C. Mao, J. Song, H. Niu, B. Jin and Y. Tian, *Appl. Surf. Sci.*, 2013, **282**, 704–708.
56 W. Zhou, X. Cao, Z. Zeng, W. Shi, Y. Zhu, Q. Yan, H. Liu, J. Wang and H. Zhang, *Energy Environ. Sci.*, 2013, **6**, 2216–2221.
57 A. Kumar, D. M. Welsh, M. C. Morvant, F. Piroux, K. A. Abbound and J. R. Reynolds, *Chem. Mater.*, 1998, **10**, 896–902.
58 S. Bhandari, M. Deepa, S. Pahal, A. G. Joshi, A. K. Srivastava and R. Kant, *ChemPlusChem*, 2010, **3**, 97–105.
59 T. H. Lee, K. Do, Y. W. Lee, S. S. Jeon, C. Kim, J. Ko and S. S. Im, *J. Mater. Chem.*, 2012, **22**, 21624–21629.